PAPER

Check for updates

Mesoporous MnOx–CeO₂ composites for NH₃-SCR: the effect of preparation methods and a third dopant†

Li Weiman, [iD] [abcd] Liu Haidi[a] and Chen Yunfa [iD] *[ad]

In this study, different preparation methods including an oxalate route, a nano-casting strategy and a traditional co-precipitation route were applied to obtain MnOx–CeO₂ mixed oxides for selective catalytic reduction (SCR) of NO with NH₃. The catalyst prepared from the oxalate route showed improved performance for NOx conversion and SO_2 + H_2O durability. To further improve the SO_2 and H_2O resistance of catalysts, ternary oxides were prepared from the oxalate route. The catalysts were studied by X-ray diffraction (XRD), Brunauer–Emmett–Teller (BET) surface area analysis, X-ray photoelectron spectroscopy (XPS), H_2 temperature-programmed reduction (H_2-TPR), NH₃ temperature-programmed desorption (NH₃-TPD), SO_2 temperature-programmed desorption (SO_2-TPD), and *in situ* diffuse reflectance infrared fourier transform spectroscopy (*in situ* DRIFTS). The nickel–manganese–cerium ternary oxide showed the best SO_2 and H_2O durability. The reason can be ascribed to its smaller pores, amorphous structure, and moderate amount of surface Mn^{3+}/oxygen species, which could decrease chemical adsorption of SO_2.

1 Introduction

Nitrogen oxides (NOx), emitted from combustion of fossil fuels in industrial stationary sources, have caused a series of environmental problems such as acid rain, haze, and ozone depletion. Selective catalytic reduction of NOx by ammonia (NH₃-SCR) is one of the most promising NOx abatement technologies. The widely used catalyst in NH₃-SCR is V_2O_5–WO_3(MoO_3)/TiO_2, whose optimum working temperature is higher than 350 °C. In practical application, the SCR reactor is usually located downstream of dust and SO_2 removing modules to avoid catalyst deactivation from dust, SO_2 and other poisoners. As a result, the temperature of flue gas is usually lower than 300 °C, and the flue gas has to be reheated to meet the V–W–Ti working temperature, which will increase the cost of deNOx. Therefore, a better choice is to develop catalysts with high deNOx efficiency, high resistance to water vapor/SO_2, and a low working temperature window.

Ce–Mn composites have been reported widely for their excellent low temperature deNOx efficiency and high N_2 selectivity. The catalytic ability of Ce–Mn composites is related to the pore structure, specific area, and redox behavior.[1–3] For example, MnOx–CeO₂ nanosphere catalyst showed superior performance compared to its counterpart MnOx–CeO₂ without any defined structural morphology.[4] MnOx–CeO₂ hollow nanotube synthesized through the interfacial oxidation–reduction reaction showed 96% NOx conversion at 100 °C, and the authors attributed to the uniform distribution of active species and the hollow porous architectures which provided huge specific surface area and sufficient acidic sites.[5] However, the activity of MnOx–CeO₂ composites is still low in the presence of SO_2 and H_2O. Lots of efforts have been done to improve SO_2 and H_2O resistance of MnOx–CeO₂ composites. For example, adding a third dopant (Sn, Cr, W, Eu *etc.*) into MnOx–CeO₂ composites can further improve the deNOx efficiency and SO_2 resistance.[6–9] Cobalt or nickel doped MnOx–CeO₂ catalysts showed high SCR activity and good tolerance of SO_2, and the authors suggested different SCR reaction pathways and mechanisms of SO_2 tolerance between Co/Ni doped and un-doped MnOx–CeO₂.[10] Mesoporous catalysts have been proved a good choice to improve SO_2 resistance.[11] Zha prepared a MnCeW catalyst on mesoporous TiO_2 spheres, and the catalyst showed excellent SCR activity in a wide temperature range.[9] Fe_2O_3 promoted halloysite-supported CeO₂–WO_3 catalysts showed improved NOx reduction in the presence of SO_2, and the authors confirmed that the increase of Brønsted acid site derived from Fe_2O_3 promotion is the main cause.[12]

[a]State Key Laboratory of Multi-phase Complex Systems, Institute of Process Engineering, Chinese Academy of Sciences, Beijing 100190, China. E-mail: chenyf@ipe.ac.cn

[b]University of Chinese Academy of Sciences, No. 19A Yuquan Road, Beijing 100049, China

[c]Zhongke Langfang Institute of Process Engineering, Langfang Economic & Technical Development Zone, Fenghua Road No. 1, Hebei Province, China

[d]CAS Center for Excellence in Urban Atmospheric Environment, Xiamen 361021, China

† Electronic supplementary information (ESI) available. See DOI: 10.1039/c9ra00731h

Based on previous studies, the catalytic performance of NH_3-SCR activity, including NOx conversion efficiency, N_2 selectivity and $H_2O + SO_2$ resistance are mainly determined by following factors: pore structure and surface area, the distribution of manganese and cerium states, and the active oxygen species including adsorbed oxygen, oxygen vacancy and lattice oxygen, as well as surface acidity. Inspired by the above studies, we have fabricated MnOx–CeO$_2$ with different pore structures by various methods, and the relationship of NH_3-SCR ability and structure was discussed. To further improve the $H_2O + SO_2$ resistance of the catalysts, nickel/cobalt was introduced to the MnOx–CeO$_2$ catalysts, and the catalytic performance was evaluated.

2 Experimental section

2.1 Catalysts preparation

All chemical reagents used in this work including $Mn(ac)_2 \cdot 4H_2O$ (99.0%), $Ce(ac)_3 \cdot 0.5H_2O$ (99.0%), $Co(ac)_2 \cdot 4H_2O$ (99.0%), $Ni(ac)_2 \cdot 4H_2O$ (99.0%), $C_2H_2O_4 \cdot 2H_2O$ (99.5%), $Mn(NO_3)_2$ (50% wt), $Ce(NO_3)_3 \cdot 6H_2O$, $Co(NO_3)_2 \cdot 6H_2O$, $Ni(NO_3)_2 \cdot 6H_2O$ and NaOH were purchased from Xilong Cop. (China) and used without further purification. To prepare MnOx–CeO$_2$ composites with different pore structures, an oxalate route, a nano-casting strategy and a simple precipitation method were applied.

In an oxalate route, calculated metal salts (the molar ratio of Mn and Ce was 6 : 4) were dissolved in deionized water at room temperature, labeled as solution A. Then, $C_2H_2O_4 \cdot 2H_2O$ (the molar ratio of $C_2H_2O_4 \cdot 2H_2O$ to total metals is 1.2) was dissolved in ethanol, labeled as solution B. The mixtures of A and B were stirred for 24 h. The precipitates were washed, dried, and finally calcined at 550 °C for 4 h. The sample was labeled as 6Mn4Ce-O. Nickel or cobalt doped MnOx–CeO$_2$ composite was prepared as the same procedure. The samples were denoted as 1Ni6Mn3Ce-O and 1Co6Mn3Ce-O, respectively.

In a nano-casting route, KIT-6 silica was employed as a hard template, and the MnOx–CeO$_2$ catalyst was synthesized by a simple "two-solvent" approach. KIT-6 silica was prepared as previously reported studies.[13] In a typical procedure, 1.0 g KIT-6 was suspended in 80 ml n-hexane and stirred at room temperature for 2 h. Then a mixed solution of $Mn(NO_3)_2$ and $Ce(NO_3)_3$ was added slowly with vigorous stirring. After stirred overnight, the mixture was filtered and dried at 80 °C for 24 h. The obtained powder was calcined at 550 °C for 4 h, with a heating rate of 2 °C min^{-1} in air. Finally, the sample was treated three times with a 2 M NaOH solution, washed to pH ∼ 7 and dried at 80 °C. The product was denoted as 6Mn4Ce-N.

As a comparison, the third MnOx–CeO$_2$ sample was synthesized by a co-precipitation method using $NH_3 \cdot H_2O$ as precipitant, and the sample was labeled as 6Mn4Ce-C.

2.2 Catalytic activity tests

Before SCR activity test, the catalysts were crushed and sieved to 40–60 mesh. A fixed-bed quartz flow reactor was used to perform SCR activity test. The typical reactant gas contained 200 ppm NOx, 200 ppm NH_3, 5%O_2, 100 ppm SO_2 (when used), 5 vol% H_2O (when used) and balance of N_2. In a typical experiment,

100 mg catalyst was used, corresponding to gas volume hourly space velocity (GHSV) of 72 000 h^{-1}. The temperature range was set to 100–300 °C. An FTIR spectrometer (Bruker Vertex 70 spectrometer, USA) equipped with a heated, multiple path gas cell (10 m) was used to collect the FTIR spectra. The NOx conversion and N_2 selectivity were calculated as follows:

$$NOx\ conversion(\%) = \frac{[NO]_{in} - [NO]_{out}}{[NO]_{in}} \times 100\%,$$

$$N_2\ selectivity(\%)$$
$$= \frac{[NO]_{in} + [NH_3]_{in} - [NO_2]_{out} - 2[N_2O]_{out}}{[NO]_{in} + [NH_3]_{in}} \times 100\%$$

2.3 Characterization

XRD patterns were recorded on a PANalytical X'Per PRO X-ray diffraction using Ni filtered Cu Kα ($\lambda = 0.15418$ nm) radiation at 40 kV and 30 mA, in 2θ from 5° to 90° with a scanning step of 0.0334°. The specific surface area and pore size distributions of all catalysts were obtained according to the Brunauer–Emmett–Teller (BET) and Barrett–Joyner–Halenda (BJH) methods, respectively, using N_2 adsorption–desorption method on an automatic surface analyzer (SSA-7300, BJ-Builder, China) at 77 K. Each sample was pre-degassed at 150 °C for 3 h. Surface species of as-prepared catalysts were determined by X-ray photoelectron spectroscopy (XPS) using a XLESCALAB 250 Xi electron spectrometer (Thermo Scientific, USA) with mono-chromatic Al Kα radiation (1486.6 eV).

H_2 temperature-programmed reduction (H_2-TPR) was conducted on a Micromeritics Chemisorb 2720 analyzer (Micromeritics, USA) at a heating rate of 10 °C min^{-1} with 5% H_2/Ar gas. The H_2 consumption was recorded continuously to investigate reduction abilities. NH_3 temperature-programmed desorption (NH_3-TPD) was performed on a Micromeritics Autochem II 2920 analyzer (Micromeritics, USA). The catalysts were firstly heated to 300 °C for 1 h in helium, and then cooled down to 50 °C. After saturated in pure NH_3 for 30 min, the samples were purged in pure helium for 1 h to remove the physically adsorbed NH_3. The TPD curve was finally recorded in helium from 50 °C to 600 °C at a heating rate of 10 °C min^{-1}. SO_2 temperature-programmed desorption (SO_2-TPD) was performed on a TP5080B apparatus (Tianjin XQ, China). 50 mg of 40–60 mesh catalysts was firstly heated to 300 °C for 1 h in 30 ml min^{-1} helium, and then cooled to 200 °C. The catalysts was saturated in 2000 ppm SO_2 for 1 h, and then purged with 30 ml min^{-1} helium for 1 h to remove residue SO_2 at 200 °C. At last, the catalyst was heated from 200 °C to 850 °C in helium at 10 °C min^{-1}.

A Bruker Vertex 70 spectrometer (Bruker, USA) equipped with diffuse reflectance accessory (PIKE, and MCT/A detector cooled by liquid nitrogen) was used for recording the *in situ* DRIFT spectra of the samples. Twenty mg KBr powder was placed under proper amount of samples, and a specially made steel stick was used to smash the sample to a flat surface. The

sample was pretreated at 300 °C for 2 h in N_2 (50 ml min^{-1}). The reaction system was cooled to 200 °C in N_2, and the spectra were collected as background. The spectra were recorded by accumulating 32 scans at a resolution of 4 cm^{-1}.

3   Results and discussion

3.1   NH₃-SCR performance

All composites prepared by different methods were tested for NH₃-SCR in temperature range of 100–350 °C, as shown in Fig. 1A. The NOx conversion of all catalysts first increased and then decreased. The NOx conversion rates at the whole temperature range of the three catalysts followed the sequence of 6Mn4Ce-O > 6Mn4Ce-C > 6Mn4Ce-N. The NOx conversion of 6Mn4Ce-O reached its maximum of 99% at ~170 °C; and it's NO conversion rate remained >80% at the temperature range of 120–275 °C. The NOx conversion of 6Mn4Ce-C was slightly lower than that of 6Mn4Ce-O. The catalyst prepared from nanocasting route showed the worst catalytic performance. Resistance to H_2O and SO_2 is an important factor that to be concerned in the evaluation of NH₃-SCR catalysts, as there is more or less SO_2 and H_2O in gas that to be managed. The H_2O + SO_2 resistance of three samples is shown in Fig. 1B. After H_2O + SO_2 was introduced into flue gas, the NOx conversion rate of

6Mn4Ce-O, 6Mn4Ce-N and 6Mn4Ce-C deceased to ~70%, ~62.5% and ~59%, respectively. This indicated that different structure of catalysts had a profound effect on resistance of H_2O and SO_2.

Addition of transition metal oxides (CrOx,[14] NiO,[10,15–17] Co₃O₄,[10] SnO₂,[18,19] et al.) into MnOx or CeO₂ were shown to improve the SCR activity in presence of SO_2 and H_2O, by increasing the surface acidity concentration of Lewis or Brønsted acid sites.[16,18,20] Based on above results, the H_2O and SO_2 resistance of sample prepared from oxalate route was better than other two samples. Therefore, we prepared Co/Ni doped MnOx–CeO₂ composites by oxalate route to further improve their resistance to H_2O and SO_2. As shown in Fig. 1C, addition of nickel or cobalt can both increase the NOx conversion rate at temperature range of 100–280 °C. For example, the NOx conversion of 1Ni6Mn3Ce-O and 1Co6Mn3Ce-O were 99% at 200 °C, slightly higher than that of 6Mn4Ce-O (~96% at 200 °C). Besides, the N₂ selectivity of 6Mn4Ce-O was lower than those of 1Ni6Mn3Ce-O and 1Co6Mn3Ce-O (Fig. 1C). The above results showed that addition of nickel or cobalt slightly improves the SCR activity and N₂ selectivity. The H_2O and SO_2 resistance of transition metal oxide doped composites were shown in Fig. 1D. With co-existence of H_2O and SO_2, NOx conversion decreased sharply to 70%, 80% and 20% over 6Mn4Ce-O, 1Ni6Mn3Ce-O
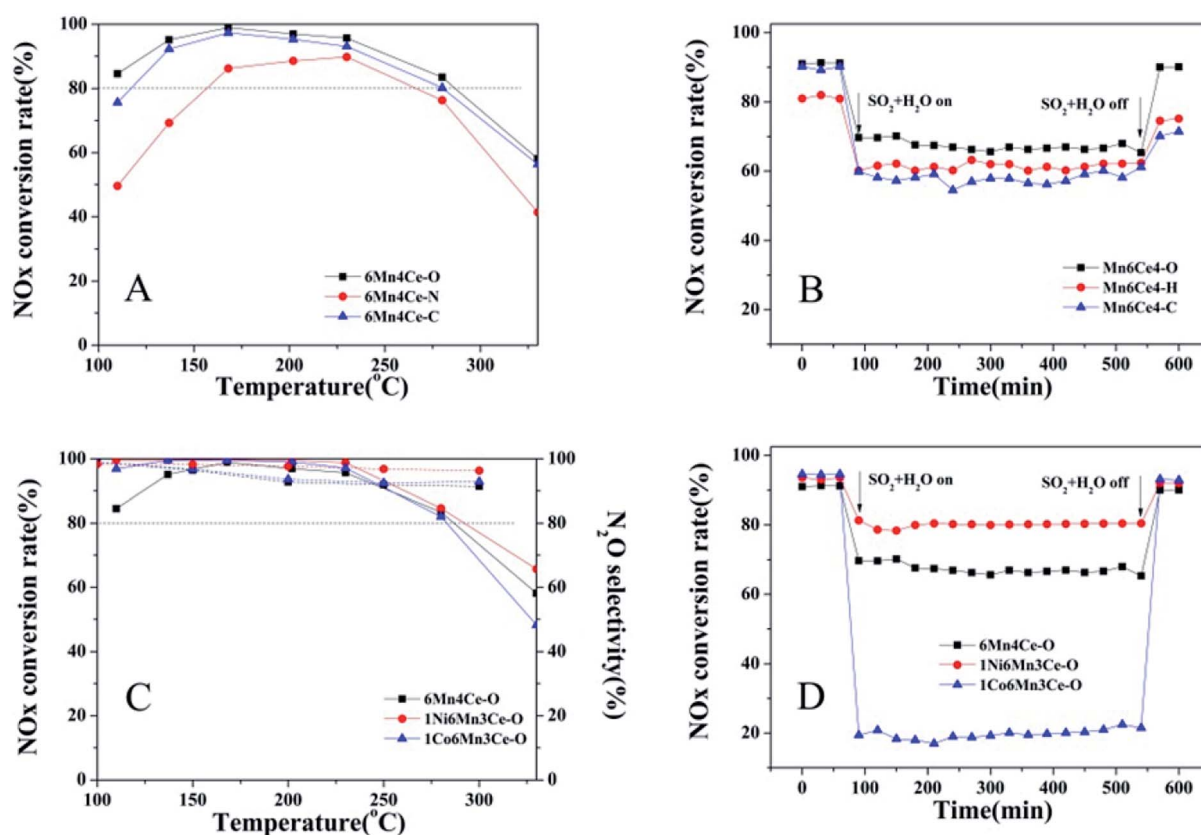

Fig. 1   (A) NOx conversion as a function of temperature over MnOx–CeO₂ prepared by different methods; (B) H_2O + SO_2 resistance over prepared by different methods at 200 °C; (C) NOx conversion as a function of temperature over nickel/cobalt doped MnOx–CeO₂; (D) H_2O + SO_2 resistance over nickel/cobalt doped samples by oxalate method at 200 °C; (reaction conditions: [NOx] = [NH₃] = 200 ppm, [O₂] = 5 vol%, [SO₂] = 100 ppm, [H₂O] = 5 vol% (when used), N₂ as balance gas, flow rate = 100 ml min^{-1}, GHSV = 60 000 h^{-1}).

Paper

RSC Advances

and 1Co6Mn3Ce-O, respectively. When H_2O and SO_2 were cutoff, the deNOx activity of 6Mn4Ce-O, 1Ni6Mn3Ce-O and 1Co6Mn3Ce-O resumed. In previous studies, MnOx–CeO_2 composite exhibited low SO_2 tolerance because of sulfate species formation. Therefore, many efforts have been done to improve the SO_2 resistance of MnOx–CeO_2 catalysts. For example, novel MnOx–CeO_2 nano-sphere catalyst showed improved SO_2 tolerance than MnOx–CeO_2 catalyst without defined structural morphology.[4] CeO_2–MnOx showed relatively good resistance to SO_2 because of its core–shell structure.[21] In our study, both preparation methods and addition of a third dopant were help to improve the resistance to SO_2 and H_2O. This phenomenon illustrated structure, as well as different interaction among third dopants and Mn–Ce composites may play important roles in NH_3-SCR, which will further be discussed in following parts.

3.2 Structural properties

3.2.1 XRD and BET analysis. The XRD patterns of all samples were shown in Fig. 2. The diffraction peaks of 6Mn4Ce-O mainly represented CeO_2 (JCPDF#34-0394) and Mn_2O_3 (JCPDF#41-1442). While the diffraction peaks of 6Mn4Ce-N and 6Mn4Ce-C exhibited broad reflections of CeO_2, no obvious peaks related to MnOx.

The diffraction peaks of 1Ni6Mn3Ce-O and 1Co6Mn3Ce-O exhibited broad reflections of CeO_2, no obvious peaks related to MnOx, NiO or cobalt oxides. Similar results[22] were reported in the case of Ni(0.4)–MnOx spinel. It is commonly accepted than amorphous structure is easy to embed and intercalate protons rapidly,[23] therefore promoting adsorption/desorption and redox reaction on the surface of catalysts.[23,24] In our study, although the deNOx efficiency and N_2 selectivity of catalysts were similar, the SO_2 + H_2O resistance varied a lot. It can be concluded that amorphous structure caused by addition of a third dopant may be responsible for the good performance of catalysts.

The N_2-adsorption–desorption isotherms and corresponding Barrett–Joyner–Halenda (BJH) pore size distribution curves for catalysts were shown in Fig. 3 (inset). The isotherms of all catalysts showed a characteristic type IV pattern, with a hysteresis loop of type H_2 in the IUPAC classification, indicating the existence of meso-pores and micro-pores. At low P/P_0, the isotherm curve of 6Mn4Ce-O had a relatively lower slope than those of other catalysts, indicating its higher degree of crystallinity, consistent with XRD results. As shown in Fig. 3 (A, inset) and Table 1, the specific surface area of 6Mn4Ce-N (152.116 m^2 g^{-1}) was higher than 6Mn4Ce-O (116.678 m^2 g^{-1}) and 6Mn4Ce-C (77.269 m^2 g^{-1}); while the pore diameter followed the sequence of 6Mn4Ce-N < 6Mn4Ce-O < 6Mn4Ce–C. This result showed that the specific surface area is not positively correlated with the NOx conversion, similar to the report from Qi.[25] Mesoporous materials present lots of edges and corners for adsorption of reactants; and the pores facilitate mass transfer at the gas–solid phase boundary.[26] Large surface area contributed more active sites, which would facilitate the adsorption of reactants. However, the SO_2 and H_2O in flue gas may also occupy the active sites of catalysts, leading to a drop of SCR conversion. The smaller pores in catalysts from oxalate routes may possibly inhibit the reaction of NOx, NH_3 with SO_2 and H_2O. Although 6Mn4Ce-O has a higher degree of crystallinity, which may not facilitate the synergistic effect between elements, the smaller pores in it can balance its structure.

For catalysts from a same oxalate route, a third dopant did not change the specific surface area significantly as shown in Table 1. However, the pore diameter of 6Mn4Ce-O and 1Co6Mn3Ce-O were among 1.5–2.5 nm. While for 1Ni6Mn3Ce-O, the pore size distribution was among 1.5–2 nm and 2.5–10 nm, similar to previous study.[27] This indicated addition of nickel into MnOx–CeO_2 could change its pore structure, leading to a combination of macropores and mesopores. According to literature,[28] the release of gaseous H_2O and COx will create pores during the decomposition of oxalate chains chelated in corresponding precursors. In our study, nickel may regulate gas release during the thermo-decomposition precursors.

3.2.2 Surface composition analysis. The XPS results were shown in Fig. 4, and all spectra were calibrated with C1s (284.8
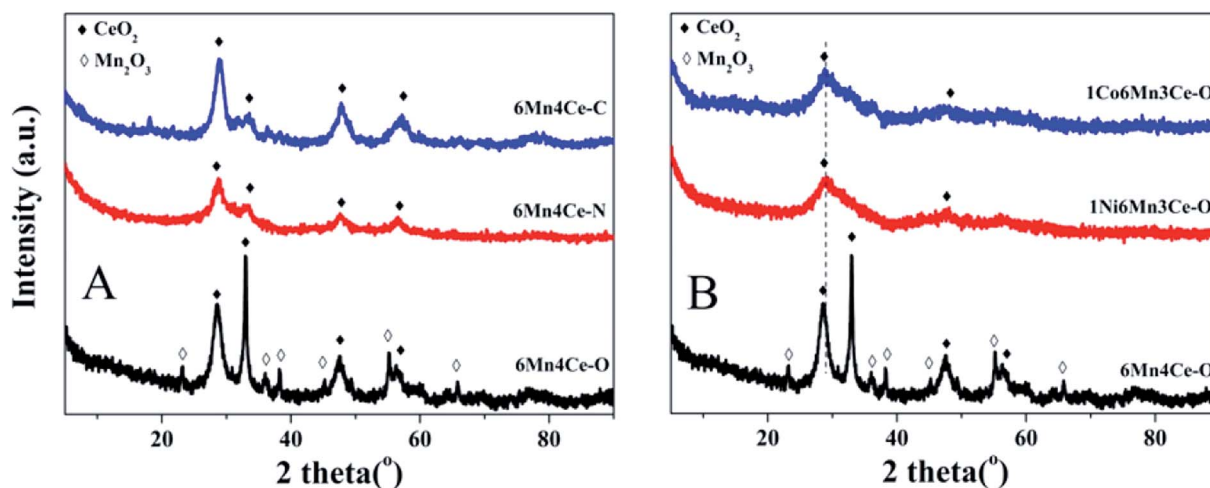

Fig. 2 XRD patterns of as-prepared samples, (A) samples from different methods, and (B) nickel or cobalt doped samples from oxalate route.
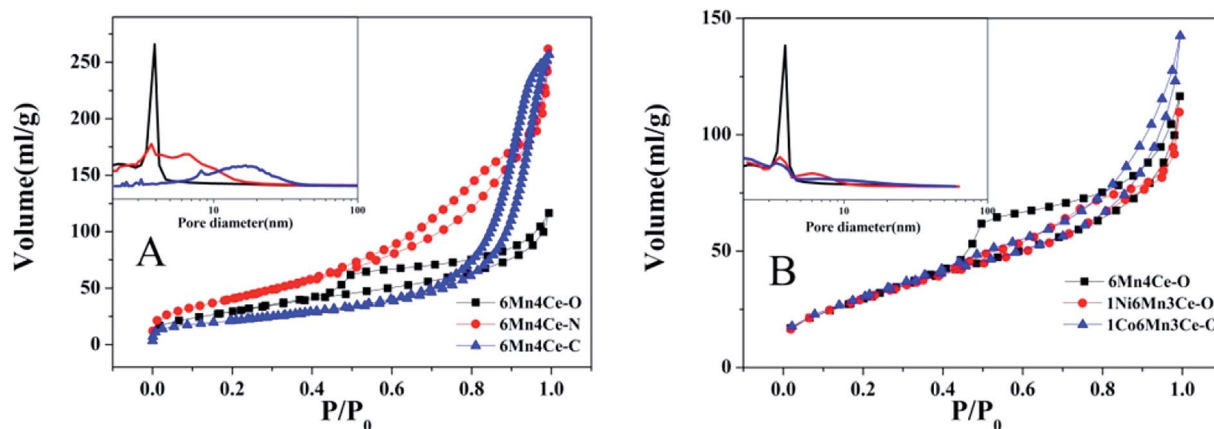
Fig. 3 N_2 adsorption/desorption isotherms and pore size distribution (inset) for samples (A) samples from different methods, and (B) nickel or cobalt doped samples from oxalate route.

Table 1 The structural data for all catalysts

	BET (m^2 g^{-1})	Pore volume (ml g^{-1})	Average pore diameter (nm)
6Mn4Ce-O	116.678	0.1686	6.5
6Mn4Ce-N	152.116	0.3955	10.7
6Mn4Ce-C	77.269	0.4036	20.6
1Ni5Mn4Ce-O	113.258	0.1428	6.0
1Co5Mn4Ce-O	116.926	0.1937	7.5

eV) before analysis. O1s spectra were fitted into two peaks. The peak centered at ~529.2–529.7 eV was related to surface lattice oxygen (denoted as O_{latt}), and the peak at higher binding energy (~532.4 eV) was ascribed to surface chemisorbed oxygen (including adsorbed oxygen, hydroxyl and carbonate, denoted as O_{ads}). Compared with 6Mn4Ce-O and 6Mn4Ce-N, the O_{latt} peak of 6Mn4Ce-C shifted to lower binding energy (529.7 eV to 529.2 eV). This phenomenon indicated that different synthesis method can regulate element valence. The relative ratios of O_{ads}/O_{latt} were 1.96, 1.26 and 1.09 for 6Mn4Ce-O, 6Mn4Ce-N and 6Mn4Ce–C, respectively. O_{ads} are considered as the active sites for SCR, because they can provide acid sites to adsorb NH_3 to form NH_4^+ or NH_3(ads).[29] From this point of view, more O_{ads} species lead to improved activity and good H_2O and SO_2 durability. The H_2O and SO_2 durability sequence of 1Ni5Mn3Ce-O, 6Mn4Ce-O, and 1Co6Mn3Ce-O was consistent with O_{ads}/O_{latt} ratio (1Ni5Mn3Ce-O > 6Mn4Ce-O > 1Co6Mn3Ce-O). Again, this indicated oxalate route and introduction of nickel leading to more surface defects. Previous studies have convinced that surface chemisorbed oxygen were more active to oxidize NO than lattice oxygen. And the higher ratio of surface chemisorbed oxygen facilitate the "fast-SCR" reaction.[10]

The Mn2p spectra were deconvoluted into three peaks located at 641.0, 642.4 and 643.8 eV, which can be assigned to Mn^{2+}, Mn^{3+} and Mn^{4+}, respectively.[30,31] The percentage of Mn species with different valences was calculated, and the results were shown in Table 2. Although a higher oxidation state of manganese species was better for redox properties,[32] moderate

ratio of Mn^{3+}/Mn^{4+} was help to improve $SO_2 + H_2O$ resistance. In our study, the surface Mn^{3+} species was related to $SO_2 + H_2O$ resistance. As shown in Table 2, the sequence of Mn^{3+} species was 6Mn4Ce-O > 6Mn4Ce-N > 6Mn4Ce-C, consistent with catalytic sequence in Fig. 1B. For samples from oxalate route, the sequence of Mn^{3+} species was 1Ni6Mn4Ce-O > 6Mn4Ce-O > 1Co6Mn4Ce-O, indicating a third dopant can regulate the surface manganese species. Based on the above various characterization studies, it was observed that different preparation method or a third dopant can regulate interaction among Mn, Ce, Ni/Co oxides, which would bring about an appropriate content of active Mn^{3+} and oxygen species on the surface of catalyst.

3.2.3 Temperature programming. Redox properties are crucial for the NH_3-SCR activities, and H_2-TPR spectra were employed to investigate redox properties of the catalysts. The H_2 consumption as a function of reaction temperature was shown in Fig. 5. For 6Mn4Ce-O, three reduction peaks were observed. The peak centered at 286 °C could be assigned to reduction of $Mn^{4+} \rightarrow Mn^{3+}$, and the peak centered at 243 °C could be ascribed to $Mn^{3+} \rightarrow Mn^{2+}$. The broad peak at 381 °C was related to the reduction of surface oxygen of CeO_2 ($Ce^{4+} \rightarrow Ce^{3+}$).[33] There was no significant peaks related to $Mn^{3+} \rightarrow Mn^{2+}$ for samples prepared from nano-casting route and co-precipitation route, consistent with XPS and XRD results, indicating their less portion of Mn^{3+}. While for 1Ni6Mn3Ce-O and 1Co6Mn3Ce-O, all peaks shifted to lower temperature range, indicating the incorporation of Ni/Co, Mn and Ce enhances the reducibility of catalyst.

NH_3-TPD was employed to investigate NH_3 adsorption, therefore to examine the acidic sites on different catalysts, as presented in Fig. 6. There were two main peaks on all spectra. The peak at the mid-temperature range (100–400 °C) is related to the desorption of NH_3 coordinated to Lewis acid sites, and the peak at high-temperature range (400–550 °C) is considered to the desorption of NH_3 coordinated to Brønsted acid sites.[15,34] Compared with catalysts prepared from nano-casting and precipitation method, the peak related to Lewis acid sites of
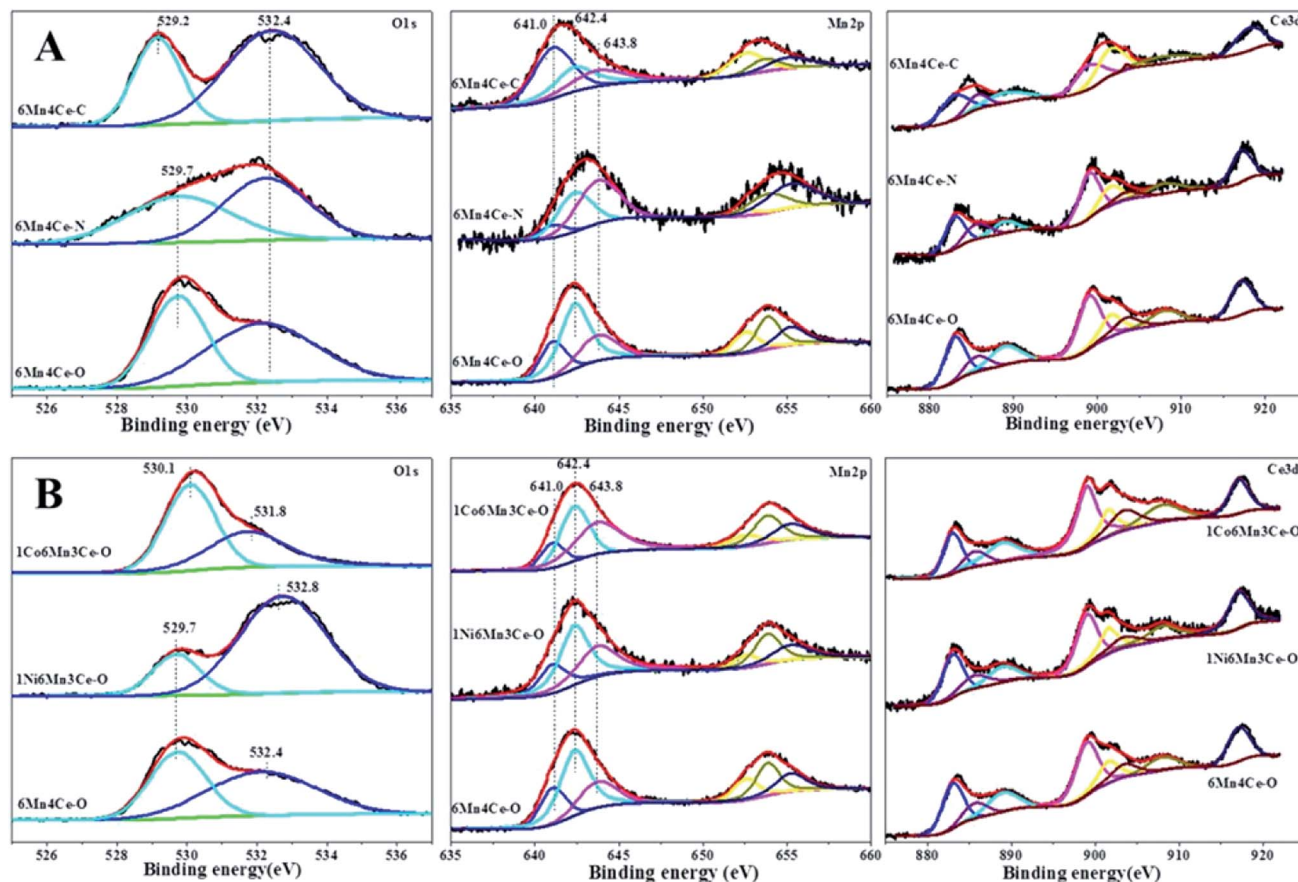
Fig. 4 O1s, Mn2p and Ce3d spectra of (A) samples from different methods, and (B) nickel or cobalt doped samples from oxalate route.

Table 2 The relative ratio of different elements for all catalysts

	O_{ads}/O_{latt}	Mn^{2+} (%)	Mn^{3+} (%)	Mn^{4+} (%)	B/L
6Mn4Ce-O	1.96	21.89	55.34	22.77	0.47
6Mn4Ce-N	1.26	9.17	39.08	51.75	0.37
6Mn4Ce-C	1.09	47.31	30.17	22.52	0.29
1Ni5Mn4Ce-O	3.91	20.64	46.73	32.63	0.95
1Co5Mn4Ce-O	0.71	14.56	39.98	45.46	0.39

6Mn4Ce-O moved toward lower temperature range, indicating the existence of weak Lewis adsorption sites. As described above, samples from oxalate route may have more acidic sites during the decomposition of precursors. The ratios of NH_3 adsorption on Brønsted acid site to Lewis acid sites of different catalysts are shown in Table 2. Oxalate route was easier to produce more Brønsted acid sites than other two methods. And addition of nickel can greatly increase the ratio of Brønsted acid/Lewis acid sites. Based on the above various characterization studies, it was observed that different preparation method or a third dopant could regulate interaction among Mn, Ce, Ni/ Co oxides, which would bring about an appropriate content of active Mn^{3+} and oxygen species on the surface of catalyst.

As samples from the oxalate route had different resistance to SO_2 and H_2O, SO_2-TPD tests were performed on these three

samples, and the results were shown in Fig. 7. There were two main desorption peaks in the temperature range of 300–600 °C, and 650–800 °C, labeled as 1 and 2, respectively. The small and broad peak in area 1 was reported to be assigned to desorption of SO_2 adsorbed on the surface of catalysts.[35] In this paper, the area labeled 1 of 1Ni5Mn4Ce was slightly smaller than the other two catalysts, which indicated less SO_2 adsorption on it. The main peak at 650–580 °C was associated to desorption of SO_2 released from the decomposition of metal sulfates. The area 2 of 1Ni5Mn4Ce was much smaller compared with others, which indicated nickel adding can inhabit formation of metal sulfates. Similar conclusion could be achieved from the TG-DTA test of samples after $SO_2 + H_2O$ resistance experiments, as shown in ESI.†

3.3 In situ DRIFTs

To better understand gas adsorption on different catalysts from oxalate route, in situ DRIFTs was conducted, and the results were shown in Fig. 8. Fig. 8A showed in situ DRIFTS spectra of $NH_3 + O_2$ adsorbed on three samples. The bands at 1235, 1565, 1610 cm^{-1} were ascribed to NH_3 coordinated on Lewis acid sites.[36] The band at 1457 cm^{-1} was due to the symmetric bending vibration of NH_4^+ chemosorbed on the Brønsted acid sites.[18] Meanwhile, a band at 3230 cm^{-1} was due to the N–H stretching vibrations of the NH_4^+.[37] Comparing with 1Co6Mn3Ce-O, 6Mn4Ce-O and 1Ni6Mn3Ce-O revealed more
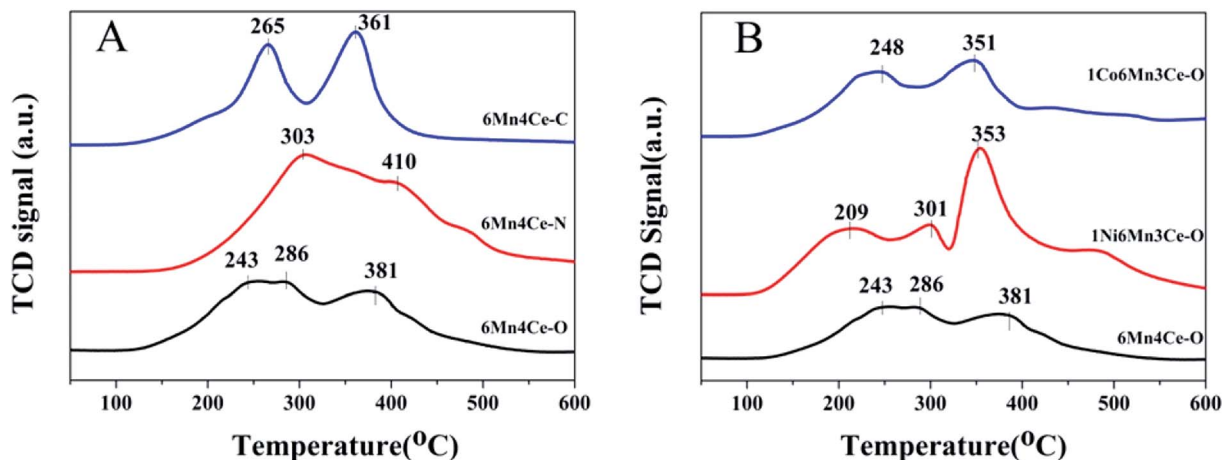
Fig. 5   H$_2$-TPR spectra of (A) samples from different methods, and (B) nickel or cobalt doped samples from oxalate route.
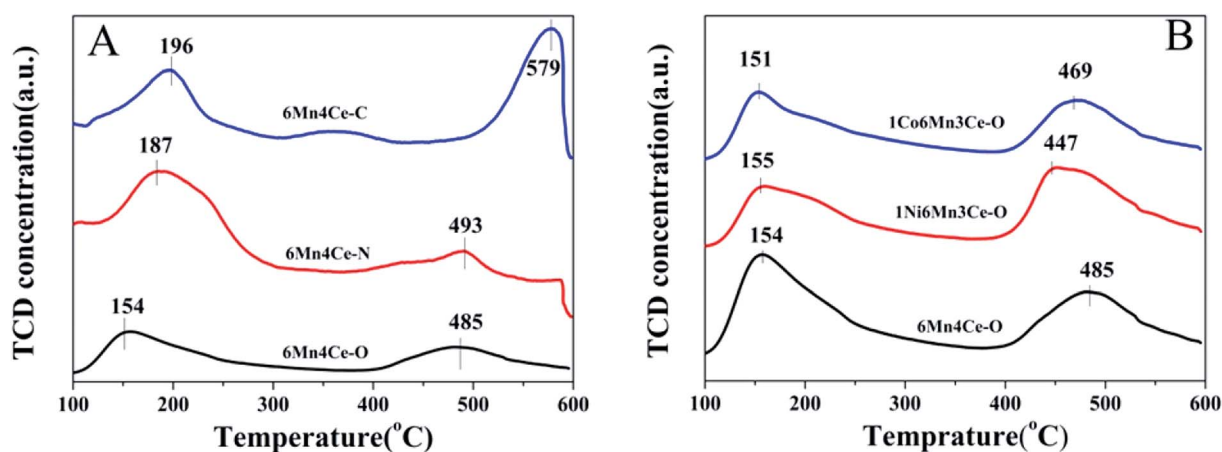

Fig. 6   NH$_3$-TPD spectra of (A) samples from different methods, and (B) nickel or cobalt doped samples from oxalate route.

Brønsted acid sites, consistent with NH$_3$-TPD results. Wu obtained the same result that addition of nickel could significantly improve the Brønsted acid sites on FeVO$_4$/TiO$_2$.[38]
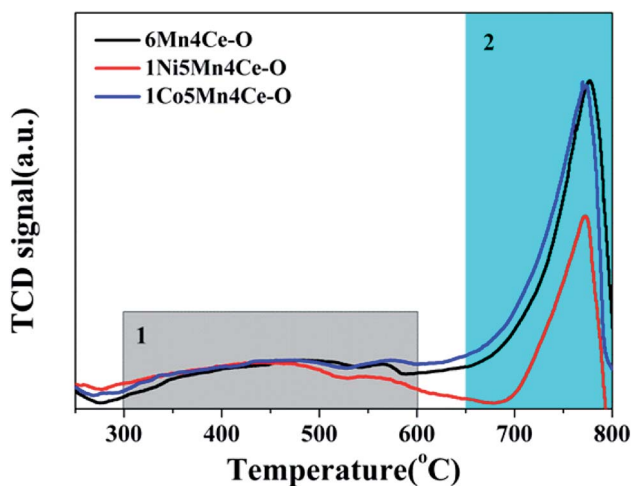

Fig. 7   SO$_2$-TPD spectra samples from an oxalate route.

Fig. 8B displayed the *in situ* DRIFTs spectra of NOx + O$_2$ adsorption on catalysts at 200 °C. The peaks centered at 1606 cm^{-1} can be ascribed to bridging monodentate nitrates, and peaks centered at 1267, 1209, 1568 and 1540 cm^{-1} were assigned to bidentate nitrates.[39] It was noteworthy that bidentate nitrates species on 1Ni6Mn3Ce-O were more than those on other catalysts, indicating nickel addition increased NO uptake. However, cobalt doping leaded to the decrease of bands related to bidentate nitrates, indicating its suppression to NO adsorption.

As 1Ni6Mn3Ce-O showed the best H$_2$O and SO$_2$ resistance, the *in situ* DRIFTs were further displayed to understand the mechanism, and the results were shown in Fig. 9. The 1Ni6Mn3Ce-O was firstly exposed to NH$_3$ for 60 min, and then SO$_2$ and H$_2$O was introduced to the reaction gas. The bands corresponding to NH$_3$(a) was quickly diminished, and new bands related to SO$_2$ adsorption appeared, as shown in Fig. 9A. While 1Ni6Mn3Ce-O was firstly exposed to NO + O$_2$ for 60 min, and then SO$_2$ was introduced to the reaction gas, no new bands appeared, which indicated that NO was more easily adsorbed on the surface of catalysts. The 1Ni6Mn3Ce-O was exposed to NH$_3$ + NO + O$_2$ at 200 °C for 60 min, and there were peaks related to
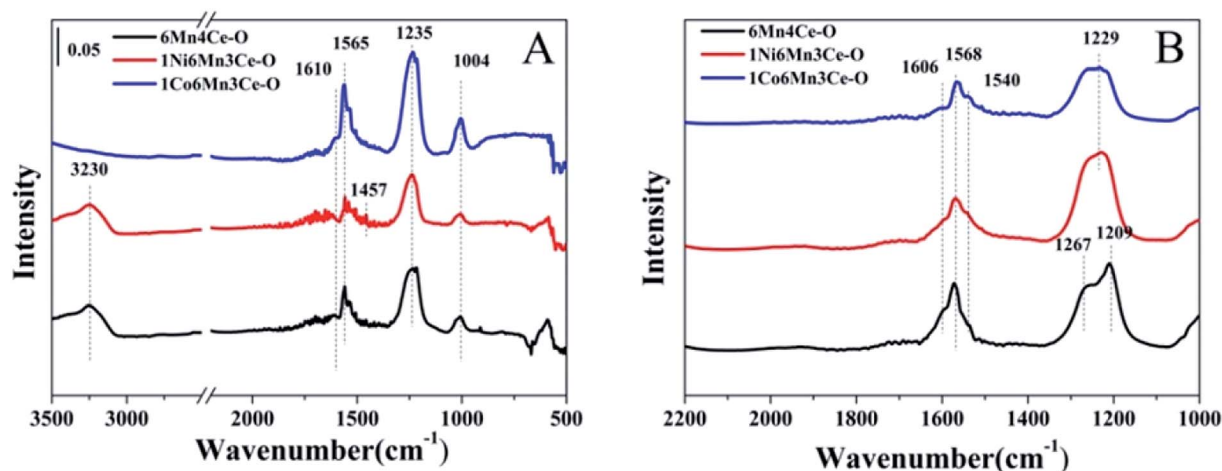
Fig. 8 *In situ* DRIFTS of samples under NH_3 + air (A) and NOx + air (B) for 1 h and then purged by helium for 30 min at 200 °C.
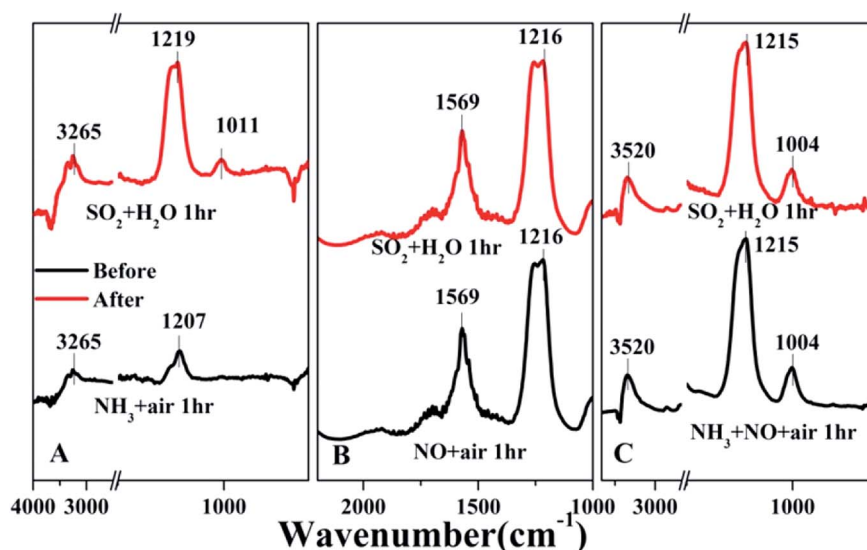

Fig. 9 *In situ* DRIFTS of 1Ni6Mn3Ce-O under NH_3 + air (A), NOx + air (B) and NOx + NH_3 + O_2 (C) for 1 h and then SO_2 and H_2O were introduced into the mixed gas for 1 h at 200 °C.

NH_3 and NOx adsorption, indicating the co-adsorption of NH_3 and NOx. After 100 ppm SO_2 and H_2O were added for another 60 min, no new bands appeared and the intensity of the original bands remained unchanged. This indicated that SO_2 and H_2O in the flue gas had no impact on NH_3-SCR of 1Ni6Mn3Ce-O, which was in agreement with the results in Fig. 1. The NH_3-SCR reaction on 1Ni6Mn3Ce-O may follow L–H mechanism, $NH_3(a)$ and NO(a) reacted to form N_2 and H_2O. When SO_2 and H_2O were introduced into the flue gas, NO(a) was more prone to react with $NH_3(a)$ than SO_2. All of these contribute to excellent H_2O and SO_2 resistance.

4   Discussion and conclusions

It was commonly accepted that there was an intense correlation between catalytic performance and structural properties, such as morphologies, crystal plans, crystal phases and porous structures. A porous structure provided much surface area and makes the adsorption and diffusion of reactant molecules easy to conduct on the surface of catalysts. In this report, catalysts with different pore structures were created by oxalate route, nanocasting strategy and co-precipitation method. Based on above analysis, catalyst from oxalate route showed best NOx conversion, including NOx conversion and SO_2 and H_2O resistance. Catalyst from oxalate route presented proper ratio of Mn^{3+}, surface oxygen species, surface acidic sites, moderate pore size and specific surface area.

Because the catalytic process over single oxide catalysts was limited, the addition of another component into the system would be favorable.[28] In this study, cobalt or nickel was added to Mn–Ce composites, which enhanced the interaction between different elements. However, the deNOx performances of

catalysts were varied based on the added elements. The introduction of nickel leads to the co-existence of Lewis acid sites and Brønsted acid sites. Addition of cobalt leads to much more Lewis acid sites. It has been proved in previous analysis that Brønsted acid sites are better for the resistance of H_2O and SO_2.

Several methods have been developed to reduce the poisonous effect of H_2O and SO_2 to SCR, such as selecting most active support, metal modification, rational design of structure and morphology,[1] and pre-sulfation.[40,41] The mechanism of these methods was to make a balance among redox properties, effective acid sites, and the formation/decomposition of ammonium sulfate, therefore enhancing the deNOx properties and suppressing the blocking effect of H_2O and SO_2. In this study, introducing nickel into Mn–Ce composite gave rise to more Brønsted acid sites, which was responsible for good H_2O and SO_2 resistance.

Different preparation method including oxalate route, nanocasting strategy and traditional co-precipitation were applied to obtain MnO_x–CeO_2 mixed oxides. The mesoporous Mn–Ce base catalysts prepared from oxalate route showed high deNOx efficiency and good SO_2 and H_2O resistance in the low temperature range. A third dopant such as nickel or cobalt was introduced to the composite to increase SO_2 and H_2O durability. The nickel–manganese–cerium ternary oxides showed the best SO_2 and H_2O durability. The reason can be ascribed to its smaller pores and amorphous structure and proper amount of surface Mn^{3+}/oxygen species, which could decrease the chemical adsorption of SO_2.

Conflicts of interest

There are no conflicts to declare.

Acknowledgements

References

1 C. Gao, J. W. Shi, Z. Y. Fan, G. Gao and C. M. Niu, Sulfur and Water Resistance of Mn-Based Catalysts for Low-Temperature Selective Catalytic Reduction of NOx: a Review, *Catalysts*, 2018, **8**, 11.

2 L. Q. Chen, F. L. Yuan, Z. B. Li, X. Y. Niu and Y. J. Zhu, Synergistic effect between the redox property and acidity on enhancing the low temperature NH_3-SCR activity for NOx removal over the $Co_{0.2}Ce_xMn_{0.8-x}Ti_{10}$ (x=0-0.40) oxides catalysts, *Chem. Eng. J.*, 2018, **354**, 393–406.

3 X. Hu, L. Huang, J. Zhang, H. Li, K. Zha, L. Shi, *et al.*, Facile and template-free fabrication of mesoporous 3D nanosphere-like $Mn_xCo_{3-x}O_4$ as highly effective catalysts for low temperature SCR of NOx with NH_3, *J. Mater. Chem. A*, 2018, **6**, 2952–2963.

4 L. Li, B. Sun, J. Sun, S. Yu, C. Ge, C. Tang, *et al.*, Novel MnO_x-CeO_2 nanosphere catalyst for low-temperature NH_3-SCR, *Catal. Commun.*, 2017, **100**, 98–102.

5 C. Li, X. Tang, H. Yi, L. Wang, X. Cui, C. Chu, *et al.*, Rational design of template-free MnO_x-CeO_2 hollow nanotube as deNOx catalyst at low temperature, *Appl. Surf. Sci.*, 2018, **428**, 924–932.

6 H. Chang, J. Li, X. Chen, L. Ma, S. Yang, J. W. Schwank, *et al.*, Effect of Sn on MnO_x-CeO_2 catalyst for SCR of NOx by ammonia: Enhancement of activity and remarkable resistance to SO_2, *Catal. Commun.*, 2012, **27**, 54–57.

7 J. Liu, R.-t Guo, M.-y Li, P. Sun, S.-m. Liu, W.-g. Pan, *et al.*, Enhancement of the SO_2 resistance of Mn/TiO_2 SCR catalyst by Eu modification: A mechanism study, *Fuel*, 2018, **223**, 385–393.

8 Z. Liu, X. Feng, Z. Zhou, Y. Feng and J. Li, Ce-Sn binary oxide catalyst for the selective catalytic reduction of NOx by NH_3, *Appl. Surf. Sci.*, 2018, **428**, 526–533.

9 K. Zha, S. Cai, H. Hu, H. Li, T. Yan, L. Shi, *et al.*, In Situ DRIFTS Investigation of Promotional Effects of Tungsten on MnO_x-CeO_2/meso-TiO_2 Catalysts for NOx Reduction, *J. Phys. Chem. C*, 2017, **121**, 25243–25254.

10 F. Gao, X. Tang, H. Yi, J. Li, S. Zhao, J. Wang, *et al.*, Promotional mechanisms of activity and SO_2 tolerance of Co- or Ni-doped MnO_x-CeO_2 catalysts for SCR of NOx with NH_3 at low temperature, *Chem. Eng. J.*, 2017, **317**, 20–31.

11 K. Zha, L. Kang, C. Feng, L. Han, H. Li, T. Yan, *et al.*, Improved NOx reduction in the presence of alkali metals by using hollandite Mn–Ti oxide promoted Cu-SAPO-34 catalysts, *Environ. Sci. Nano*, 2018, **5**, 1408–1419.

12 L. Kang, L. Han, J. He, H. Li, T. Yan, G. Chen, *et al.*, Improved NOx Reduction in the Presence of SO_2 by Using Fe_2O_3-Promoted Halloysite-Supported CeO_2–WO_3 Catalysts, *Environ. Sci. Technol.*, 2019, **53**, 938–945.

13 F. Kleitz, S. Hei Choi and R. Ryoo, Cubic Ia3d large mesoporous silica: synthesis and replication to platinum nanowires, carbon nanorods and carbon nanotubes, *Chem. Commun.*, 2003, 2136–2137.

14 H. Liu, L. Wei, R. Yue and Y. Chen, CrO_x–CeO_2 binary oxide as a superior catalyst for NO reduction with NH_3 at low temperature in presence of CO, *Catal. Commun.*, 2010, **11**, 829–833.

15 J. Liu, X. Li, R. Li, Q. Zhao, J. Ke, H. Xiao, *et al.*, Facile synthesis of tube-shaped Mn-Ni-Ti solid solution and preferable Langmuir-Hinshelwood mechanism for selective catalytic reduction of NOx by NH_3, *Appl. Catal., A*, 2018, **549**, 289–301.

16 Y. Wan, W. Zhao, Y. Tang, L. Li, H. Wang, Y. Cui, *et al.*, Ni-Mn bi-metal oxide catalysts for the low temperature SCR removal of NO with NH_3, *Appl. Catal., B*, 2014, **148–149**, 114–122.

17 X. Li, Y. Du, X. Guo, R. Wang, B. Hou and X. Wu, Synthesis of a Novel NiMnTi Mixed Metal Oxides from LDH Precursor

and Its Catalytic Application for Selective Catalytic Reduction of NOx with NH$_3$, *Catal. Lett.*, 2018, **149**, 456–464.

18 H. Chang, X. Chen, J. Li, L. Ma, C. Wang, C. Liu, *et al.*, Improvement of Activity and SO$_2$ Tolerance of Sn-Modified MnOx-CeO$_2$ Catalysts for NH$_3$-SCR at Low Temperatures, *Environ. Sci. Technol.*, 2013, **47**, 5294–5301.

19 B. Thirupathi and P. G. Smirniotis, Co-doping a metal (Cr, Fe, Co, Ni, Cu, Zn, Ce, and Zr) on Mn/TiO$_2$ catalyst and its effect on the selective reduction of NO with NH$_3$ at low-temperatures, *Appl. Catal., B*, 2011, **110**, 195–206.

20 X. Tang, J. Li, L. Wei and J. Hao, MnOx-SnO$_2$ catalysts synthesized by a redox coprecipitation method for selective catalytic reduction of NO by NH$_3$, *Chin. J. Catal.*, 2008, **29**, 531–536.

21 S. Li, B. Huang and C. Yu, A CeO$_2$-MnOx core-shell catalyst for low-temperature NH$_3$-SCR of NO, *Catal. Commun.*, 2017, **98**, 47–51.

22 L. Chen, X. Niu, Z. Li, Y. Dong, Z. Zhang, F. Yuan, *et al.*, Promoting catalytic performances of Ni-Mn spinel for NH$_3$-SCR by treatment with SO$_2$ and H$_2$O, *Catal. Commun.*, 2016, **85**, 48–51.

23 W. Sun, X. Li, Q. Zhao, M. Tade and S. Liu, W$_\alpha$Mn$_{1-\alpha}$Ox Catalysts Synthesized by a One-Step Urea Co-precipitation Method for Selective Catalytic Reduction of NOx with NH$_3$ at Low Temperatures, *Energy Fuels*, 2016, **30**, 1810–1814.

24 N. Fang, J. Guo, S. Shu, H. Luo, Y. Chu and J. Li, Enhancement of low-temperature activity and sulfur resistance of Fe$_{0.3}$Mn$_{0.5}$Zr$_{0.2}$ catalyst for NO removal by NH$_3$-SCR, *Chem. Eng. J.*, 2017, **325**, 114–123.

25 G. Qi and R. T. Yang, Performance and kinetics study for low-temperature SCR of NO with NH$_3$ over MnOx–CeO$_2$ catalyst, *J. Catal.*, 2003, **217**, 434–441.

26 M. Qiu, S. Zhan, H. Yu and D. Zhu, Low-temperature selective catalytic reduction of NO with NH$_3$ over ordered mesoporous Mn$_x$Co$_{3-x}$O$_4$ catalyst, *Catal. Commun.*, 2015, **62**, 107–111.

27 P. Zhang, Y. Sun, W. Su, Y. Wei and J. Liu, Low-temperature selective catalytic reduction of NO with NH$_3$ over Ni-Mn-Ox catalysts, *RSC Adv.*, 2016, **6**, 107270–107277.

28 W. Tang, Y. Deng, W. Li, J. Li, G. Liu, S. Li, *et al.*, Importance of porous structure and synergistic effect on the catalytic oxidation activities over hierarchical Mn-Ni composite oxides, *Catal. Sci. Technol.*, 2016, **6**, 1710–1718.

29 B. Jia, J. Guo, H. Luo, S. Shu, N. Fang and J. Li, Study of NO removal and resistance to SO$_2$ and H$_2$O of MnOx/TiO$_2$, MnOx/ZrO$_2$ and MnOx/ZrO$_2$–TiO$_2$, *Appl. Catal., A*, 2018, **553**, 82–90.

30 Q. Shen, L. Zhang, N. Sun, H. Wang, L. Zhong, C. He, *et al.*, Hollow MnOx-CeO$_2$ mixed oxides as highly efficient catalysts in NO oxidation, *Chem. Eng. J.*, 2017, **322**, 46–55.

31 W. Sun, X. Li, Q. Zhao, J. Mu and J. Chen, Fe–Mn Mixed Oxide Catalysts Synthesized by One-Step Urea-Precipitation Method for the Selective Catalytic Reduction of NOx with NH$_3$ at Low Temperatures, *Catal. Lett.*, 2018, **148**, 227–234.

32 D. S. Zhang, L. Zhang, L. Y. Shi, C. Fang, H. R. Li, R. H. Gao, *et al.*, In situ supported MnOx-CeOx on carbon nanotubes for the low-temperature selective catalytic reduction of NO with NH$_3$, *Nanoscale*, 2013, **5**, 1127–1136.

33 Y. Niu, T. Shang, S. Hui, X. Zhang, Y. Lei, Y. Lv, *et al.*, Synergistic removal of NO and N$_2$O in low-temperature SCR process with MnOx/Ti based catalyst doped with Ce and V, *Fuel*, 2016, **185**, 316–322.

34 J. Liu, X. Li, Q. Zhao, J. Ke, H. Xiao, X. Lv, *et al.*, Mechanistic investigation of the enhanced NH$_3$-SCR on cobalt-decorated Ce-Ti mixed oxide: In situ FTIR analysis for structure-activity correlation, *Appl. Catal., B*, 2017, **200**, 297–308.

35 L. Chen, R. Li, Z. Li, F. Yuan, X. Niu and Y. Zhu, Effect of Ni doping in NixMn1-xTi10 (x = 0.1-0.5) on activity and SO$_2$ resistance for NH$_3$-SCR of NO studied with in situ DRIFTS, *Catal. Sci. Technol.*, 2017, **7**, 3243–3257.

36 H.-D. Liu, W.-M. Li, R.-L. Yue and Y.-F. Chen, Reaction Mechanism of NH$_3$-Selective Catalytic Reduction for NO on CrOx-CeO$_2$ Binary Oxide, *Chin. J. Inorg. Chem.*, 2013, **29**, 2399–2404.

37 T. Zhang, F. Qiu, H. Chang, Y. Peng and J. Li, Novel W-modified SnMnCeOx catalyst for the selective catalytic reduction of NOx with NH$_3$, *Catal. Commun.*, 2017, **100**, 117–120.

38 G. Wu, X. Feng, H. Zhang, Y. Zhang, J. Wang, Y. Chen, *et al.*, The promotional role of Ni in FeVO$_4$/TiO$_2$ monolith catalyst for selective catalytic reduction of NOx with NH$_3$, *Appl. Surf. Sci.*, 2018, **427**, 24–36.

39 W. Shan, F. Liu, H. He, X. Shi and C. Zhang, Novel cerium-tungsten mixed oxide catalyst for the selective catalytic reduction of NOx with NH$_3$, *Chem. Commun.*, 2011, **47**, 8046–8048.

40 K. Wijayanti, S. Andonova, A. Kumar, J. Li, K. Kamasamudram, N. W. Currier, *et al.*, Impact of sulfur oxide on NH$_3$-SCR over Cu-SAPO-34, *Appl. Catal., B*, 2015, **166**, 568–579.

41 L. Zhang, H. Qu, T. Du, W. Ma and Q. Zhong, H$_2$O and SO$_2$ tolerance, activity and reaction mechanism of sulfated Ni–Ce–La composite oxide nanocrystals in NH$_3$-SCR, *Chem. Eng. J.*, 2016, **296**, 122–131.